We are IntechOpen, the world's leading publisher of Open Access books Built by scientists, for scientists

4,800
Open access books available

122,000
International authors and editors

135M
Downloads

Our authors are among the

154
Countries delivered to

TOP 1%
most cited scientists

12.2%
Contributors from top 500 universities

CLARIVATE ANALYTICS BOOK CITATION INDEX INDEXED

WEB OF SCIENCE™

Selection of our books indexed in the Book Citation Index in Web of Science™ Core Collection (BKCI)

Interested in publishing with us?
Contact book.department@intechopen.com

Numbers displayed above are based on latest data collected.
For more information visit www.intechopen.com

Chapter 13

β-FeOOH/TiO_2 Heterojunction for Visible Light-Driven Photocatalytic Inactivation of *E. coli*

Mahabubur Chowdhury, Ncumisa Mpongwana, Franscious Cummings, Veruscha Fester and Seteno Ntwampe

Additional information is available at the end of the chapter

http://dx.doi.org/10.5772/62893

Abstract

In this work, we report on the photocatalytic properties of β-FeOOH/TiO_2 heterojunction material for the inactivation of *Escherischia coli*. XRD, HRTEM, EELS, ELNEFS were used to characterize the as-prepared material. A log reduction of the initial bacterial population was achieved after 45 min of irradiation in the presence of 0.1 mL of hydrogen peroxide. The enhanced photocatalytic activity was due to the effective charge transfer between Ti^{4+}, Fe^{3+}, and O^{2+} as shown from the EELS analysis of the heterojunction structure. The role of various reactive species formed due to the photocatalytic reaction was also investigated. Presence of •OH radicals in the bulk solution was the key factor in the photocatalytic inactivation of *E. coli*.

Keywords: photocatalysis, heterojunction structure, microbial inactivation, *E. coli* , charge transfer

1. Introduction

Risk associated with waterborne diseases such as typhoid, hepatitis A and E, polio, diarrhoea, and cholera are increasing in developing countries due to shortages of clean and safe drinking water [1]. Various chemical and physical treatment processes have been used to disinfect drinking water. Chlorination is a widely used method to disinfect water. However, chlorination can be problematic as it reacts with naturally occurring organic compounds in water to produce carcinogenic by-products such as trihalomethanes (THMs) and haloacetic acids (HAAs)

[2]. Ozonation is another method that is used to disinfect water [1]. On the other hand, ozonation is an energy intensive technique which can be proved to be costly in many developing countries. Physical separation process like thermal destruction at elevated temperatures and membrane filtration of pathogens is effective but not economically feasible. Water disinfection by UV radiation can also be utilized. Conversely, the use of direct and intensive UV radiation possesses health hazards. Hence, its application is limited within the special medical and laboratory purposes only [3, 4]. Therefore, new techniques are required to control the spread of microorganisms in water due to the complications related to different water disinfection processes [4]. Photocatalysis is a promising method that can be used to disinfect water cheaply, as the energy required to activate photocatalytic reaction can be obtained freely from the sun. In the presence of light, electron (e^-) - hole (h^+) pairs are generated due to band gap photoexcitation of photocatalyst (semiconductors) [5]. The photo generated (e^-)-(h^+) pairs are capable of oxidising organic matter either directly or indirectly by reacting with solvents or additives to generate highly nonselective reactive species, hydroxide radicals (•OH) [5–7]. Photocatalysis is an environmentally benign process as the ultimate by-product of the treatment process is carbon dioxide and water.

Since the discovery of water splitting by Fujishima and Honda using TiO_2, there has been an explosion of various studies on TiO_2 as a photocatalyst [8]. TiO_2 is generally considered as nontoxic, photocorrosion resistant, and inexpensive photocatalyst [5]. One of the biggest drawback of TiO_2 as photocatalyst is that it can only utilise photon from near UV light range to generate electron (e^-) - hole (h^+) pairs due to its very large band gap (3.2 eV) [6, 9]. The UV region is only 4% in the solar spectrum. Hence, a large amount of sunlight is unexploited in TiO_2 photocatalysis processes. Because of this, designing of efficient visible-light driven (VLD), TiO_2-based photocatalyst is of importance from energy, environment, and economic point of view. Various TiO_2-based VLD photocatalyst has been developed up to date [9–14]. Most of the developed catalyst has been tested for the degradation of organic pollutants. There is a scarcity of literature in the application of VLD photocatalyst for the inactivation of microorganisms in water. A great deal of effort should be given in improving the efficiency of photocatalytic inactivation of microorganisms to prevent the outbreak of waterborne diseases and to cope with the future energy and environmental challenges [4].

The efficacy of the VLD photocatalyst depends on the efficient separation of charge carriers. Formation of heterojunction between TiO_2 and other oxide materials have has been proven to be an effective way of enhancing the efficiency of photocatalysis process under visible light [6, 9, 10, 15]. Besides the band potential matching of the semiconductors, ability to conduct (e–) – (h^+) pairs in the respective electron and hole accepting semiconductors are very important in the formation of a heterojunction structure [6, 10]. In our previous work [6], we have prepared β-FeOOH/TiO_2 heterojunction for photocatalytic degradation of textile effluent. However, the photocatalytic efficiency of the heterojunction for microorganism inactivation has not been evaluated, despite a strong correlation between antimicrobial effect and organic compounds degradation effect [4, 16]. Within this view, we report on the photocatalytic inactivation of microorganisms by using β-FeOOH/TiO_2 heterojunction as a VLD photocatalyst. *Escherischia coli* was used as a target microorganism. Hydrogen peroxide was used as a

http://dx.doi.org/10.5772/62893

green electron scavenger to increase the photocatalytic inactivation efficiency of the VLD photocatalyst.

2. Materials and Methods

Analytical grade reagents, without any further purifications, were used in all preparation methods. $FeCl_3.6H_2O$, NH_4OH, EtOH, hydrogen peroxide (30% V/V), isopropanol, sodium oxalate, Cr(VI), and Degussa-P25 were purchased from Sigma Aldrich South Africa.

2.1. Catalyst preparation

Nanorod-shaped β-FeOOH particles were synthesised according to the previously reported method [17, 18]. Typical synthesis process consists of adding certain amount of $FeCl_3.6H_2O$ in a solution of equal amount of water and EtOH (V/V). The final pH of the solution was kept at ~2. 200 mL of the solution was placed in a Teflon lined autoclave. The autoclave was slowly heated to 100°C and was kept at that temperature for 2 h; then followed by washing and centrifuging of the precipitated sample once the autoclave cooled down naturally. The sample were dried in a desiccator.

The method of heterojunction formation between TiO_2 and P25 was adopted from previously reported study [6, 19, 20]. Maleic acid was used as an organic binder to form a chemically bonded interface between TiO_2 and β-FeOOH. The role of maleic acid was, to anchor the TiO_2 on the surface of β-FeOOH through its dicarboxylic functional group [21]. In a typical synthesis procedure, an appropriate amount of β-FeOOH nanorods were dispersed in 30 mL of EtOH. In a separate beaker, a gram of P25 powder was dispersed in 30 ml of EtOH. Maleic acid of 0.1 M concentration (10 mL) was added to the β-FeOOH suspension. Both solutions were stirred for 4 h. After 4 h, the TiO_2 suspension was added to the β-FeOOH suspension and stirred for 12 h. The mixture was washed and centrifuged several times. The samples were dried in an oven at 60°C. The dried samples were calcined at 300°C. The calcined samples were further treated by UV irradiation for 4 h.

2.2. *E. coli* cell preparation

Single colony of *E. coli* bacterial cells was taken from the stock and incubated in 10% nutrient broth solution at 37°C for 18 h with shaking. Certain amount of culture was washed with saline and centrifuged at 2000 rpm for 5 minute. The supernatant solution was discarded, and the bacterial pellet was re-suspended in sterile saline solution.

2.3. Photocatalytic inactivation of *E. coli*

The photocatalytic inactivation of *E. coli* was carried in a homemade jacketed glass reactor. A catalyst load of 0.02 g was added to 100 mL of deionised water and placed in the reactor. A 300 W halogen tungsten lamp was used as a visible light source. The halogen tungsten lamp was placed inside a cooling jacket. The circulating water in the cooling jacket placed around

the halogen tungsten lamp minimised the heat generation due to infrared light emitted from the halogen lamp and also acted as a UV filter. The lamp with the cooling jacket was submerged in the 100 mL catalyst suspension placed in the glass reactor under stirring. The solution temperature was always found to be ~30°C. Hydrogen peroxide (0.1 mL) was Used as a green electron scavenger. A Li-CORE LI-250A light metrer coupled with quantum photosynthetically active radiation PAR (PARphotosynthetically active radiation) sensor was used to measure the photosynthetic photon flux density (PPFD) emitted from the halogen tungsten lamp. The PPFD emitted from the halogen tungsten light source was measured to be 1 X× 10^4 μmols^{-1}. It was assumed that the number of incident photons reaching the catalyst surface will be constant throughout the reactor because of homogeneous suspension around lamp. A working cell suspension was obtained by serially diluting the stock microbial solution and adding 1 mL of the solution to the 100 mL catalyst suspension. An initial concentration of ~300 CFU/mL of *E. coli* was used for all the experiments reported in this study. Sample from the reactor was withdrawn at regular interval and centrifuged to separate the solid catalyst. The supernatant solution was diluted with sterilized solution. An appropriate amount of diluted sample was spread in agar solution and incubated at 37°C for 24 h. The number of viable cells was determined by counting the number of the colonies formed. All experiments were conducted in triplicates.

2.4. Characterization of the material

A Phillips PW 3830/40 Generator with Cu-Kα radiation was used to determine the X-ray diffraction patterns of the heterojunction structure for phase identification purposes. High resolution transmission electron microscopy (HR-TEM) was performed using a Tecnai F20 FEG-TEM, equipped with a Gatan Image Filter (GIF2001) for morphology evaluation and also electron energy loss spectroscopy (EELS) and energy-filtered TEM (EFTEM) analysis. Plural scattering and the contribution from low low-energy plasmon losses were eliminated by applying a power law background -shape to each spectrum.

3. Results and discussion

3.1. β-FeOOH/TiO_2 heterojunction characterization

Degusa P25, a mixture of anatase and rutile, was used as TiO_2 material. Hence, both anatase (JCPDS card no: 71–1167) and rutile (JCPDS card no: 75–1748) peaks could be observed from the XRD patterns of TiO_2 (Data not shown). **Figure 1a** presents TEM Micrographs of TiO_2. Selected area electron diffraction pattern (**Figure 1b**) shows that the TiO_2 is predominantly anatase as the first four diffracting planes indicates. High-resolution TEM micrograph viewed along the [001] direction (Inset **Figure 1a**), allowed for direct measurement of the lattice constants and found to be value of $a = b = 0.378$ nm, as determined for the tetragonal crystal structure. A value of 0.944 nm was calculated for lattice constant c from the SAED pattern (1b). TEM image of the pristine β-FeOOH nanorods (JCPDS No. 42–1315) is presented in **Figure 1c**. TEM image of the β-FeOOH/TiO_2 heterojunction material is presented in **Figure 1e**. It can be

http://dx.doi.org/10.5772/62893

seen from **Figure 1e** that tight contacts between particles have been formed. Interestingly no rod-shaped β-FeOOH/TiO_2 particles were found in the heterojunction structure. Transformation of rod shaped β-FeOOH to pseudo spherical particles in chemically bonded interface between β-FeOOH and TiO_2 has been well documented in our earlier work [6]. **Figure 1d** presents the EDS of the heterojunction structure. The presence of Fe and Ti signal in the EDS is a signature of the formation of a composite structure. Further evaluation of heterojunction formation between β-FeOOH and TiO_2 was done by electron energy loss-filtered transmission electron microscopy (EFTEM). Formation of interface between β-FeOOH and TiO_2 in the composite material can be clearly seen from the EFTEM images EFTEM images (**Figure 1 f–h**).

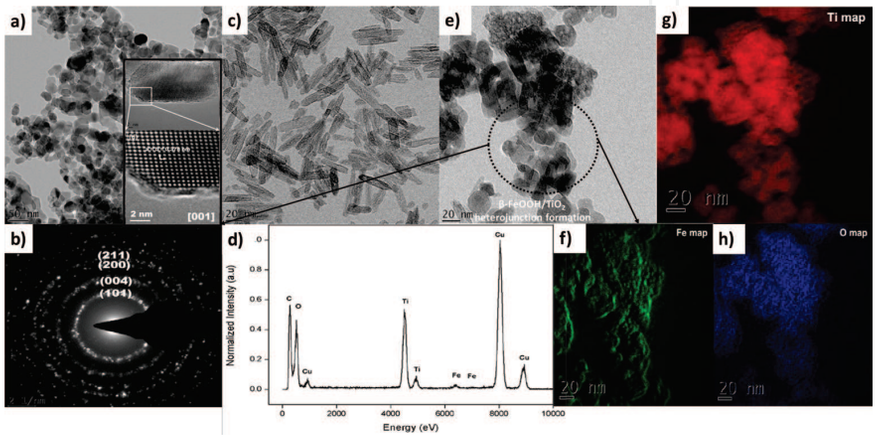

Figure 1. (a) TEM image of pristine P25 material, (b) SAED pattern of the pristine P25 material, (c) TEM image of pristine β-FeOOH nanorods, (d & and, e) TEM image and corresponding EDS of the β-FeOOH/TiO_2 heterojunction structure, and (f, g, –h) elemental X-ray mapping of the composite structure.

Anatase and rutile both have Ti^{4+} valency as well as a tetragonal crystal structure. However, rutile contains six atoms per unit cell whereas anatase has twelve. In either polymorph, each Ti atom is coordinated to six O atoms, whereas each O atom is coordinated to three Ti atoms, thereby forming a perfect TiO_6 octahedron. These octahedra are slightly slanted in both anatase and rutile, with two Ti-O distances being 0.1 Å greater in length compared to the other four bond lengths. This is accompanied by a deviation from 90° of the O-Ti-O angles. Subsequently, the local point-group symmetry is lowered around the Ti atom from O_h to D_{2h} in rutile and D_{2d} in anatase. Anatase and rutile differ as a result of secondary coordination during which the TiO_6 octahedra are joined together by sharing two edges in rutile and four in anatase [22, 23]. A study of the molecular orbital (MO) energy level diagram of rutile [24] shows that the two lowest unoccupied orbitals separate into a threefold t_{2g} and twofold e_g orbital, commonly known as the crystal-field orbitals. In ideal O_h symmetry, they consist of two distinct levels; however, with the lowering of the symmetry in rutile, t_{2g} orbital splits into b_{3g}, a_g, and b_{2g} sub-orbitals, whereas the e_g orbital morphs into b_{1g} and a_g sub-levels. Tight-binding theory [25] shows that the electronic band structure for rutile exhibits $L_{2,3}$ ionization edges in the conduction band, which are basically t_{2g} and e_g levels, their maxima separated by about 4.5 eV; for anatase, the L_2 and L_3 bands are slightly closer at 3.8 eV. From **Figure 2a**, it can be seen that the $L_{2,3}$ obtained during electron energy loss maxima is separated by 5.17 eV (465.31 and 470.48

eV), with the crystal-field splitting of the L_2 and L_3 lineshapes into the respective t_{2g} and e_g subbands clearly visible, as indicated by the arrows in the inset. As determined from the SAED pattern of **Figure 1b**, the P25 particles are predominantly anatase; however, the separation of the L_3 and L_2 ionization edges of 5.17 eV suggests the presence of rutile.

Figure 2b shows the $L_{2,3}$ ionization edge of the β-FeOOH nanorods. In all iron-oxides, this lineshape is characterized by Fe 2p → 3d and 4s transitions. However, a lower probability of transition to the s orbitals exist, and hence, the Fe $L_{2,3}$ edges are comprised of mainly excitation to Fe 3d orbitals. This spin–orbit interaction separates the Fe L_3 ($2p_{3/2}$) and L_2 ($2p_{1/2}$) edges by about 13 eV. The unoccupied states in the 3d bands of the Fe atom are related to the white-line intensities. EELS of β-FeOOH shows an ionization edge onset at 708 eV, peaking at 716.58 eV for L_3, and 729.63 eV for the L_2 edge. A deconvolution of the L_3 peak shows the characteristic crystal field splitting into the t_{2g} and e_g bands. This is shown in the inset of **Figure 2b**. The L_3/L_2 ratio of 2.29 is recorded for these nanostructures.

The EELS spectrum of the composite material is shown in **Figure 2c** and compared to that of the P25 and as-synthesized β-FeOOH nanorods samples. A study of the $L_{3,2}$ ionization edge of

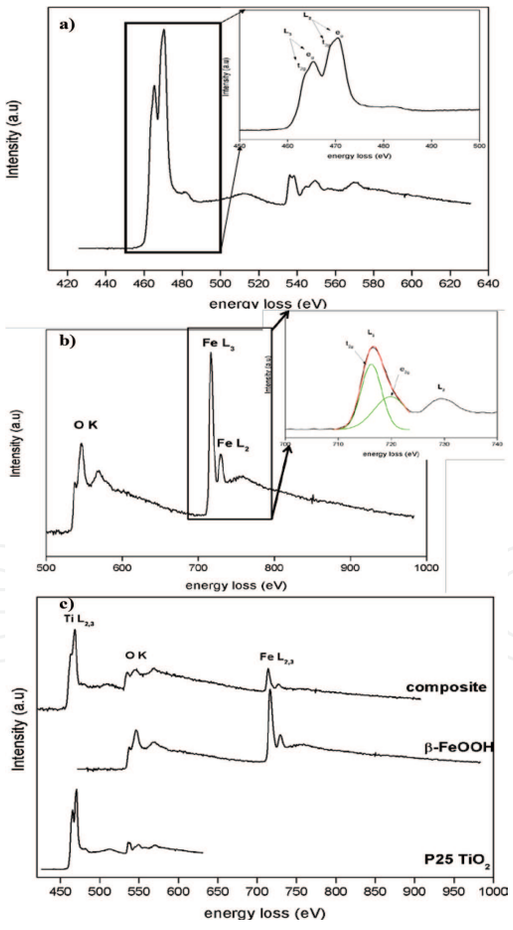

Figure 2. (a) EELS of pristine P25, (b) EELS of the Fe $L_{3,2}$ and oxygen K edges of the β-FeOOH nanorods, and (c) comparison of EELS between P25, β-FeOOH nanorods and β-FeOOH/TiO_2 heterojunction structure.

http://dx.doi.org/10.5772/62893

Ti and Fe in **Figure 2c** shows a lack of evidence of the crystal-field splitting in the Ti $L_{3,2}$ lineshape, which is accompanied by a rearrangement of the L_3/L_2 ratio of Fe to 1.65. Investigation of the O K edge shows a similar decrease in the splitting. This suggested the presence of charge transfer/bonding between the Ti^{4+}, Fe^{3+}, and O^{2+} ions during the composite synthesis.

3.2. Evaluation of photocatalytic inactivation of *E. coli*

Figure 3a presents the photocatalytic activity of the heterojunction structure under visible light. A common microorganism; i.e. that is *E. coli* was used to evaluate the inactivation efficiency of the *E. coli*. In the absence of light, the photocatalyst did not show any antimicrobial activity, implying that the heterojunction material is not toxic. It is known that UV ray can inactivate microorganisms. A halogen tungsten lamp with a water filter was used to simulate the solar irradiation. In the absence of catalyst, there was no decrease in bacterial population after 45 minutes of irradiation. Hence, the role of UV-induced disinfection of the bacterial cells can be ignored. In the presence of the catalyst and light only, no significant reduction of bacterial population was observed. The efficiency of a photocatalyst depends on the successful separation of photogenerated e^-— h^+. Hydrogen peroxide have been used in many studies as a green electron scavenger [26–28]. Hydrogen peroxide (in the presence of light only) was used to evaluate the role of hydrogen peroxide in the inactivation of *E. coli*. In the absence of catalyst (in the presence of light and hydrogen peroxide), only 0.2 log reduction of bacterial population was achieved after 45 minutes of irradiation. However, in the presence of light, catalyst and hydrogen peroxide 1 log reduction of bacterial population was achieved. This composition showed a synergistic catalytic inactivation of *E. coli*. Three different catalyst load, i.e. that is 0.01, 0.02, and 0.04 g/L, was evaluated to optimise the photocatalytic inactivation of *E. coli*. 0.5 log reduction of bacterial population was achieved in the case of 0.01 and 0.04 g/L catalyst load. A catalyst load of 0.02 g/L showed the highest photocatalytic inactivation (1 log reduction). It is well known that the presence of excessive amount of catalyst creates the screening effect which reduces the photocatalytic activity of the catalyst in a given system.

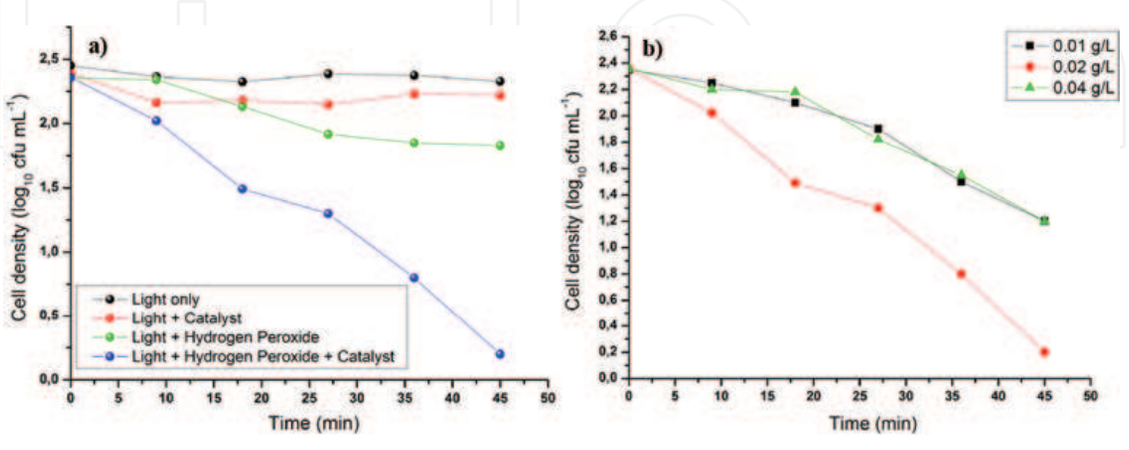

Figure 3. (a) Catalytic activity of the heterojunction structure, (b) Effect of catalyst load on photocatalytic inactivation of *E. coli*.

3.3. Photocatalytic inactivation mechanism of *E. coli*

In our previous study [6], we have showed the existence of an inter semiconductor e^-- h^+ transport mechanism in the β-FeOOH/TiO_2 heterojunction structure. This phenomenon was responsible for the enhanced photocatalytic performance of the structure. Various reactive species are, e.g. for example, •OH and $O_2^{\bullet-}$; are generated during the photocatalytic reaction [(Equations. (1)–(4)]. However, the roles of photogenerated reactive species, whether they remain bound to the surface or diffuse into the bulk solution, Were not investigated in the case of β-FeOOH/TiO_2 heterojunction structure.

$$h^+_{vb} + H_2O \rightarrow {}^{\bullet}OH + H^+ \quad (1)$$

$$H_2O_2 + e^- \rightarrow {}^{\bullet}OH + OH^- \quad (2)$$

$$H_2O_2 \xrightarrow{hv} {}^{\bullet}OH \quad (3)$$

$$O_2 + e^- \rightarrow O_2^{\bullet-} \quad (4)$$

As discussed previously, in the absence of the hydrogen peroxide, no significant reduction in bacterial population was observed. This was due to the rapid recombination of e^-- h^+ pairs. Hydrogen peroxide itself in the presence of UV (emitted from halogen tungsten lamp) generates •OH [(Equation. (3)] via photolysis. To evaluate the role of bacterial inactivation due to valence band hole, 40 μmol L^{-1}, Cr (VI) was used as an electron scavenger [4] to isolate the role of photolysis (**Figure 4**). It can be seen from **Figure 4a** that 87% of the bacterial colony was reduced. This highlights the possibility photocatalytic inactivation of *E. coli* by either •OH [(Eq.uation (1)] or $O_2^{\bullet-}$ [(Equation. (4)]. Sodium oxalate of 20 μmol L^{-1} concentration, a hole scavenger [4], was used to explore the role of $O_2^{\bullet-}$ for bacterial inactivation purpose. It can be seen from **Figure 4** that no significant reduction of bacterial population occurred in the absence of valence band hole. Hence, the contribution of $O_2^{\bullet-}$ was postulated to be minimal. So, it can be postulated that the photocatalytic inactivation of *E. coli* is mainly due to the presence •OH. To evaluate the significant •OH generation process [(between Equation (1), and 2+(3)] and its role in *E. coli* inactivation, sodium oxalate and hydrogen peroxide were added simultaneously in the solution. This was done to suppress the formation of •OH due to Equation (1). Hence, the effect of Equations (2) and (3) could be observed directly. It can be seen from **Figure 4** that the reduction in bacterial population was lower compared to when Cr(VI) was used as an electron scavenger. This demonstration postulated that there is a synergistic effect between photocatalysis and photolysis in the generation of •OH for *E. Coli coli* inactivation. Isopropanol was used as a radical quenching agent to isolate the effect of catalyst surface bound •OH or those diffusing in the solution. Isopropanol is easily oxidised by •OH and exhibits low affinity towards semiconductor surface in aqueous media as reported in previous literature [4,

http://dx.doi.org/10.5772/62893

29, 30]. Isopropanol of 15 mol L^{-1} isopropanol was used as a •OH quenching agent in the presence of hydrogen peroxide. The photocatalytic inactivation was completely inhibited in the presence of isopropanol highlighting the role of •OH in bulk solution. From the control experiments, it was established that the catalyst and the scavengers (the amount used) had no significant effect on the inactivation of *E. coli*.

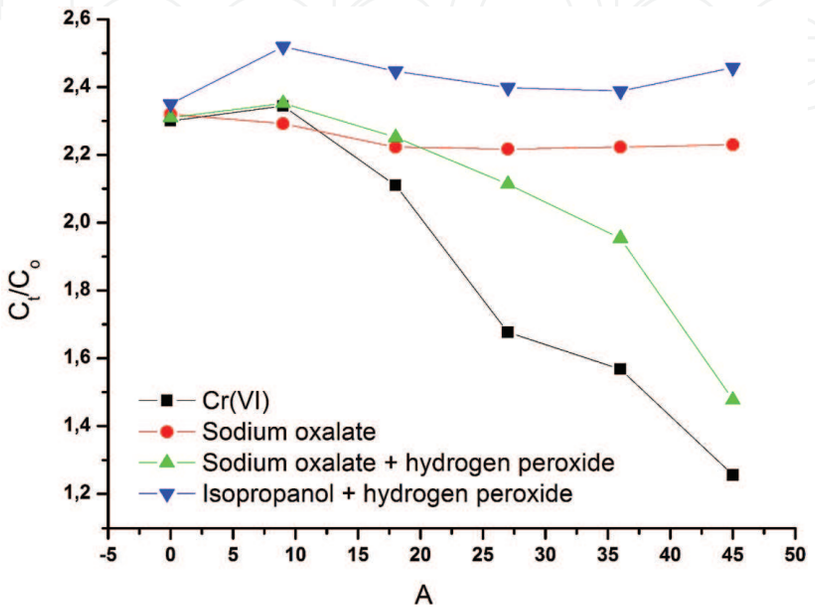

Figure 4. Role of reactive species on the photocatalytic inactivation of *E. coli*.

4. Conclusion

β-FeOOH/TiO_2 heterojunction prepared via organic linker mediated route was used for photocatalytic inactivation of *E. coli*. Controlled experiments showed that the as as-prepared catalyst had no antimicrobial properties in the absence of light. The catalyst showed good photocatalytic properties in the presence of simulated solar light and 0.1 mL of hydrogen peroxide. Hydrogen peroxide acted as a green electron scavenger to inhibit the e^-- h^+ recombination rate. Different scavenger was used to identify the role of exact reactive species in the photocatalytic disinfection of *E. Coli*. Generation of •OH via photocatalysis and photolysis and its presence in the bulk solution was the main driver behind the inactivation of *E. coli*.

Acknowledgements

This work was supported by National Research Foundation of South Africa (Grant No: 88220).

Author details

Mahabubur Chowdhury[1*], Ncumisa Mpongwana[2], Franscious Cummings[3], Veruscha Fester[1] and Seteno Ntwampe[2*]

*Address all correspondence to: chowdhurym@cput.ac.za and ntwampes@cput.ac.za

1 Flow Process and Rheology Centre, Cape Peninsula University of Technology, Cape Town, South Africa

2 Bioresource Engineering Research Group, Cape Peninsula University of Technology, Cape Town, South Africa

3 Electron Microscopy Unit, University of the Western Cape, Bellville, South Africa

References

[1] M. Vijay, K. Ramachandran, P.V. Ananthapadmanabhan, B. Nalini, B.C. Pillai, F. Bondioli, A. Manivannan, R.T. Narendhirakannan. Photocatalytic inactivation of Gram-positive and Gram-negative bacteria by reactive plasma processed nanocrystalline TiO_2 powder. Current Applied Physics, 13 (2013) 510–516.

[2] L. Liang, P.C. Singer. Factors influencing the formation and relative distribution of haloacetic acids and trihalomethanes in drinking water. Environmental Science & Technology, 37 (2003) 2920–2928.

[3] M.A. Shannon, P.W. Bohn, M. Elimelech, J.G. Georgiadis, B.J. Marinas, A.M. Mayes. Science and technology for water purification in the coming decades. Nature, 452 (2008) 301–310.

[4] L.-S. Zhang, K.-H. Wong, H.-Y. Yip, C. Hu, J.C. Yu, C.-Y. Chan, P.-K. Wong. Effective photocatalytic disinfection of *E. coli* K-12 using AgBr-Ag-Bi_2WO_6 nanojunction system irradiated by visible light: the role of diffusing hydroxyl radicals. Environmental Science & Technology, 44 (2010) 1392–1398.

[5] R. Comparelli, E. Fanizza, M.L. Curri, P.D. Cozzoli, G. Mascolo, R. Passino, A. Agostiano. Photocatalytic degradation of azo dyes by organic-capped anatase TiO_2 nanocrystals immobilized onto substrates. Applied Catalysis B: Environmental, 55 (2005) 81–91.

[6] M. Chowdhury, M. Ntiribinyange, K. Nyamayaro, V. Fester. Photocatalytic activities of ultra-small β-FeOOH and TiO_2 heterojunction structure under simulated solar irradiation. Materials Research Bulletin, 68 (2015) 133–141.

[7] A.K. Chakraborty, M.A. Kebede. Preparation and characterization of WO_3/Bi_3O_4Cl nanocomposite and its photocatalytic behavior under visible light irradiation. Reaction Kinetics, Mechanisms and Catalysis, 106 (2012) 83–98.

[8] A. Fujishima, K. Honda. Electrochemical photolysis of water at a semiconductor electrode. Nature, 238 (1972) 37–38.

[9] S.B. Rawal, S. Bera, D. Lee, D.-J. Jang, W.I. Lee. Design of visible-light photocatalysts by coupling of narrow bandgap semiconductors and TiO_2: effect of their relative energy band positions on the photocatalytic efficiency. Catalysis Science & Technology, 3 (2013) 1822–1830.

[10] S.B. Rawal, A.K. Chakraborty, Y.J. Kim, H.J. Kim, W.I. Lee. Double-heterojunction structure of $SbxSn_{1-x}O_2/TiO_2/CdSe$ for efficient decomposition of gaseous 2-propanol under visible-light irradiation. RSC Advances, 2 (2012) 622–630.

[11] B. Pal, M. Sharon, G. Nogami. Preparation and characterization of TiO_2/Fe_2O_3 binary mixed oxides and its photocatalytic properties. Materials Chemistry and Physics, 59 (1999) 254–261.

[12] J. Tokarský, P. Čapková. Structure compatibility of TiO_2 and SiO_2 surfaces. Applied Surface Science, 284 (2013) 155–164.

[13] Y. Bessekhouad, D. Robert, J.V. Weber. Bi_2S_3/TiO_2 and CdS/TiO_2 heterojunctions as an available configuration for photocatalytic degradation of organic pollutant. Journal of Photochemistry and Photobiology A: Chemistry, 163 (2004) 569–580.

[14] Y. Bessekhouad, D. Robert, J.V. Weber. Photocatalytic activity of Cu_2O/TiO_2, Bi_2O_3/TiO_2 and $ZnMn_2O_4/TiO_2$ heterojunctions. Catalysis Today, 101 (2005) 315–321.

[15] S.B. Rawal, A.K. Chakraborty, W.I. Lee. Heterojunction of FeOOH and TiO_2 for the formation of visible light photocatalyst. Bulletin of the Korean Chemical Society, 30 (2009) 2613–2616.

[16] F. Chen, X. Yang, Q. Wu. Photocatalytic oxidation of *Escherischia coli, Aspergillus niger*, and formaldehyde under different ultraviolet irradiation conditions. Environmental Science & Technology, 43 (2009) 4606–4611.

[17] M. Chowdhury, V. Fester, G. Kale. Growth kinetics evaluation of hydrothermally synthesized β-FeOOH nanorods. Journal of Crystal Growth, 387 (2014) 57–65.

[18] M. Chowdhury, V. Fester, G. Kale, O. Cespedes. Hydrothermal precipitation of β-FeOOH nanostructure(s) in mixed solvent: study of their morphological and structural evolution. Journal of Nanoparticle Research, 16 (2014) 1–11.

[19] O. Oghenochuko, M. Chowdhury, N. Kudzanai, F. Cummings, V. Fester, O.S. Fatoki. Novel β-FeOOH/NiO composite material as a potential catalyst for catalytic ozonation degradation of 4-chlorophenol. RSC Advances, 5 (2015) 59513–59521.

[20] A.K. Chakraborty, M.E. Hossain, M.M. Rhaman, K.M.A. Sobahan, Fabrication of Bi2O3/TiO2 nanocomposites and their applications to the degradation of pollutants in air and water under visible-light, Journal of Environmental Sciences, 26 (2014) 458–465.

[21] Y.J. Kim, B. Gao, S.Y. Han, M.H. Jung, A.K. Chakraborty, T. Ko, C. Lee, W.I. Lee. Heterojunction of $FeTiO_3$ nanodisc and TiO_2 nanoparticle for a novel visible light photocatalyst. The Journal of Physical Chemistry C, 113 (2009) 5.

[22] R. Brydson, H. Sauer, W. Engel, J.M. Thomass, E. Zeitler, N. Kosugi, H. Kuroda. Electron energy loss and X-ray absorption spectroscopy of rutile and anatase: a test of structural sensitivity. Journal of Physics: Condensed Matter, 1 (1989) 797.

[23] F.R. Cummings, T.F.G. Muller, G.F. Malgas, C.J. Arendse. Investigation of the growth and local stoichiometric point group symmetry of titania nanotubes during potentiostatic anodization of titanium in phosphate electrolytes. Journal of Physics and Chemistry of Solids, 85 (2015) 278–286.

[24] L.A. Grunes. Study of the K edges of $3d$ transition metals in pure and oxide form by X-ray-absorption spectroscopy. Physical Review B, 27 (1983) 2111–2131.

[25] L.A. Grunes, R.D. Leapman, C.N. Wilker, R. Hoffmann, A.B. Kunz. Oxygen K near-edge fine structure: an electron-energy-loss investigation with comparisons to new theory for selected $3d$ transition-metal oxides. Physical Review B, 25 (1982) 7157–7173.

[26] J. Li, F. Sun, K. Gu, T. Wu, W. Zhai, W. Li, S. Huang. Preparation of spindly CuO microparticles for photodegradation of dye pollutants under a halogen tungsten lamp. Applied Catalysis A: General, 406 (2011) 51–58.

[27] W. Zhai, F. Sun, W. Chen, Z. Pan, L. Zhang, S. Li, S. Feng, Y. Liao, W. Li. Photodegradation of p-nitrophenol using octahedral Cu_2O particles immobilized on a solid support under a tungsten halogen lamp. Applied Catalysis A: General, 454 (2013) 59–65.

[28] W. Zhai, F. Sun, W. Chen, L. Zhang, Z. Min, W. Li. Applications of Cu_2O octahedral particles on ITO glass in photocatalytic degradation of dye pollutants under a halogen tungsten lamp. Materials Research Bulletin, 48 (2013) 4953–4959.

[29] Y. Chen, S. Yang, K. Wang, L. Lou. Role of primary active species and TiO_2 surface characteristic in UV-illuminated photodegradation of Acid Orange 7. Journal of Photochemistry and Photobiology A: Chemistry, 172 (2005) 47–54.

[30] A. Amine-Khodja, A. Boulkamh, C. Richard. Phototransformation of metobromuron in the presence of TiO_2. Applied Catalysis B: Environmental, 59 (2005) 147–154.